ISSN: 0974-5823 Vol. 6 No. 3 December, 2021

*International Journal of Mechanical Engineering*

# Growth and characterization of organic 3-nitroacetophenone single crystals for optical applications

**P.P. Abirami Priya[a,f], T. Suthan[b,f], S. Abraham Thambi Raja[c,f*], V. Bena Jothy[d,f], G.Bagavathi Sankar[e,f]**

[a]Research Scholar (Reg. No: 11835), Department of Physics, Women's Christian College, Nagercoil – 629001, India

[b]Assistant Professor, Department of Physics, Lekshmipuram College of Arts and Science, Neyyoor-629802, India

[c]Associate Professor (Rtd), Department of Physics, Lekshmipuram College of Arts and Science, Neyyoor - 629802, India

[d]Assistant Professor, Department of Physics, Women's Christian College, Nagercoil – 629001, India

[e]Assistant Professor, Department of Physics, St.John's college of Arts and Science, Ammandivilai– 629204, India

[f]Affiliated to Manonmaniam Sundaranar University, Abishekapatti, Tirunelveli - 627012, India

**Abstract**

The nitroaromatic organic 3-nitroacetophenone single crystal was grown by slow evaporation technique by using acetone as a solvent. Single crystal XRD shows the grown crystal belongs to the monoclinic system with a centrosymmetric space group of $P2_1/n$. Powder XRD study displays the crystalline quality of the grown crystal. The presence of various functional groups is confirmed by using Fourier transform infrared (FTIR) and FT-Raman spectral analyses. The optical properties of the grown crystal were analysed by UV-Visible studies. The cut-off was obtained around 382 nm and the optical parameters are calculated. The thermal stability of the grown single crystal was analyzed by thermogravimetric (TG) and differential thermal analyses (DTA). The melting and the decomposition points are observed at 85°C and 238°C from the DTA analysis. The TG analysis shows single stage decomposition. Three well known integral approximations Coats-Redfern, Horowitz-Metzger and Broido methods are used to calculate the kinetic and thermodynamic parameters. The dielectric constant, dielectric loss, AC electrical conductivity, activation energy and various electrical parameters are determined by dielectric analysis.

**Keywords:** Organic compounds; X-ray diffraction; Vibrational analysis; Optical Properties, Thermal Properties; Electrical properties.

## 1. Introduction

Organic crystals having optical properties are increasing the interest of researchers in creating favourable photonic devices such as sensitive detectors, organic field-effect optical waveguides, optical switching, multichannel signal converters and optical logic gates. Organic compounds have a high degree of delocalization and are mostly created by weak van der Waal and hydrogen bonds. Hence, they are often more optically nonlinear than inorganic materials. The organic materials with nonlinear properties have higher second harmonic generation efficiencies and also shows significantly better laser damage thresholds . Most of the organic materials used in nonlinear optical technologies are aromatic system derivatives with donor and acceptor substitutions [1-3]. The need of electronic devices which are environment friendly is leading the demand for solution-based fabrication methods. The use of soluble organic semiconductors allows fabrication of electronic devices, such as organic light emitting diodes, organic field effect transistors (OFETs) and organic solar cells, with both low energy consumption and low cost. The absence of grain boundaries and the resulting low defect density, organic single crystals shows good performance in OFETs [4-6]. The use of biological compounds in photonic devices are recently under investigation. Acetophenone derivatives are such biological compound which shows good photochemical and biological characteristics. Nitroaromatic compounds have been broadly studied due to their interesting biological activities and their extended use in the chemical industry. The 3-nitroacetophenone is an aromatic nitro organic compound in which $NO_2$ group is attached to the aromatic ring in the meta position and its molecular formula is $C_8H_7NO_3$. The 3-nitroacetophenone is an aromatic ketone group used as fragrance in perfumes and soaps, intermediate in pharma industry, as a solvent for plastics and resins and as food flavouring agent [7-9]. The organic material 3-nitroacetophenone single crystal was successfully grown by slow evaporation method using the organic solvent acetone. The grown crystals are characterized by single crystal and powder X-ray diffraction, FTIR, FT-Raman, optical, thermal and dielectrically.

## 2. Experimental

The organic material 3-nitroacetophenone was commercially purchased. It has a molecular weight of 165.15 g/mol. 3-nitroacetophenone is insoluble in water while soluble in organic solvents. The solubility was determined by using different organic solvents like acetone, ethanol and methanol. Finally, acetone was recognized as the best solvent. The solubility of the nitroaromatic material 3-nitroacetophenone was studied by the gravimetric method for temperatures varying from 33°C to 50°C. The obtained result reveals that the solubility increases with the increase in temperature and is shown in fig.1. The solution was stirred well at room

temperature for 2 hours to obtain a clear solution and it was further purified by repeated recrystallization processes. The solution was then filtered to eradicate the impurities. The container was covered perfectly using a perforated polyethylene sheet and was allowed to crystallize at room temperature. Good quality organic 3-nitroacetophenone single crystals were grown after 20-22 days with good transparency. The grown 3-nitroacetophenone single crystal is shown in fig.2.

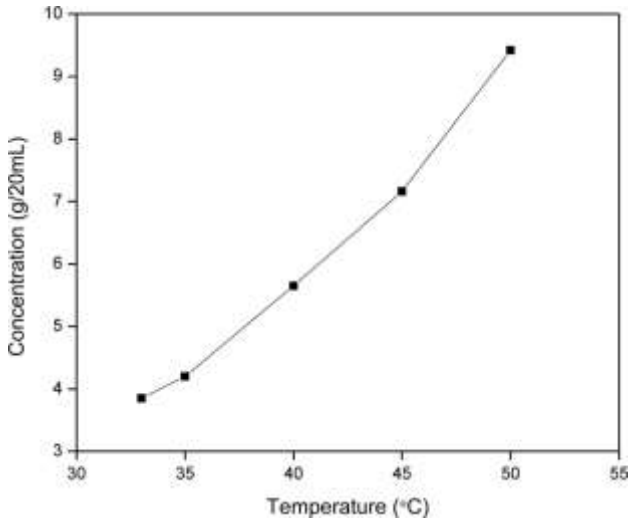


**Fig. 1 Solubility curve of 3-nitroacetophenone**

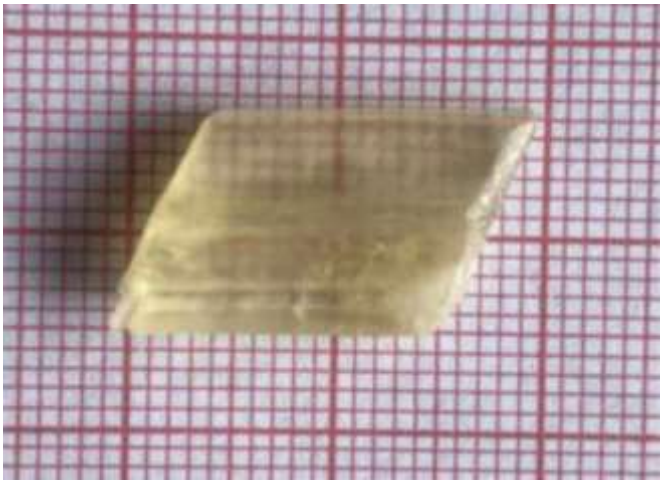

**Fig. 2 Photograph of grown 3-nitroacetophenone single crystal**

### 3. Result and discussion

### 3.1 X-ray diffraction analyses

Single crystal X-ray diffraction analysis for the grown 3-nitroacetophenone crystal has been carried out to identify the cell parameters. The single-crystal X-ray diffraction studies have been carried out using Bruker single crystal KAPPA APEX II diffractometer. The obtained lattice parameters are precisely close to the reported values [10]. The result shows that the grown 3-nitroacetophenone single crystal belongs to the monoclinic system with the centrosymmetric space group $P2_1/n$. The reported lattice parameters are compared with the obtained lattice parameters and are shown in table 1.

**Table 1**

**Single crystal XRD data for grown 3-nitroacetophenone**

| Parameter | Reported value | Present work |
|---|---|---|
| a (Å) | 7.39 | 7.48 |
| b (Å) | 9.88 | 9.98 |
| c (Å) | 10.81 | 10.77 |
| α (°) | 90 | 90 |
| β (°) | 99.59 | 99.98 |
| γ (°) | 90 | 90 |
| Volume (Å$^3$) | 779.4 | 792 |
| System | monoclinic | monoclinic |
| Space group | $P2_1/n$ | $P2_1/n$ |

The structure of the grown crystal was examined by powder XRD using PANalyticalX'Pert Pro powder X-ray with $CuK_\alpha$ radiation. The powdered sample was analyzed in the diffraction angle range from 10 to 80°. The recorded powder X-ray diffraction spectrum is shown in fig.3. The obtained (h k l) values are analyzed by using the 2θ software. The well-defined and sharp intensity peaks at definite 2θ angles reveal the fine crystalline nature of the grown 3-nitroacetophenone single crystal.

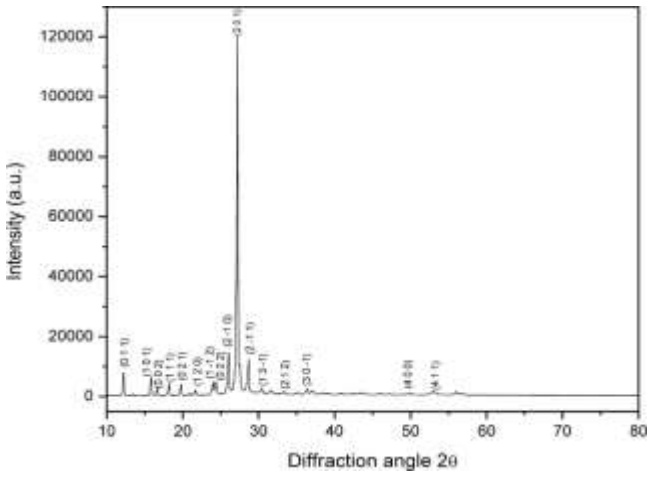


**Fig. 3 Powder XRD Pattern of 3-nitroacetophenone**

### 3.2 FTIR and FT-Raman analyses :

Infrared absorption and Raman scattering are the two main common spectroscopies used to detect the vibrations in molecules. They are used to provide information on chemical structures, physical shapes and to identify substances groups

based on their spectral patterns. Infrared absorption involve direct excitation of the molecule from ground state to excited state by a photon of exactly same energy difference between them. Raman scattering uses higher energy radiation and the difference in energy between excited state and ground state is measured by subtracting the energy of the scattered photon from the incident beam [11]. The functional groups of organic 3-nitroacetophenone single crystal are confirmed by FTIR and FT-Raman spectral analyses. The FTIR spectrum was recorded using a Perkin Elmer FTIR spectrum RIX spectrometer with KBr pellet from 4000 – 400 $cm^{-1}$. The obtained FTIR spectrum of 3-nitroacetophenone is shown in fig. 4. The FT-Raman spectrum was recorded using BRUKER: RFS 27 FT Raman spectrometer from 3500 – 50 $cm^{-1}$. The obtained FT-Raman spectrum of 3-nitroacetophenone is shown in fig. 5. The absorption peak at 3089 $cm^{-1}$in FTIR and FT-Raman is due to the aryl CH stretching vibration indicates the presence of aromatic =C-H. The strong and medium absorption peak obtained at 2965 and 2968 $cm^{-1}$ in FTIR and FT-Raman spectrum confirms the presence of methyl ketones due to CH asymmetric stretching vibration. The medium absorption peak obtained at 2924 $cm^{-1}$ in FTIR and the strong absorption peak obtained at 2925 $cm^{-1}$ in FT-Raman confirms the presence of methyl ketones due to CH symmetric stretching vibration. The two absorption peaks observed at 1614, 1577 $cm^{-1}$ in FTIR spectrum and FT-Raman spectrum are due to the aromatic ring quadrant stretching vibrations. The intensity peak at 1526 $cm^{-1}$ in FTIR and 1522 $cm^{-1}$ in FT-Raman indicates the presence of aromatic nitro compounds due to asymmetric $NO_2$ stretching vibration. The absorption peak at 1349 $cm^{-1}$ and 1348 $cm^{-1}$ in FTIR and FT-Raman spectrum are due to symmetric $NO_2$ stretching, indicates the presence of aromatic meta substituted nitro compound. Also the strong absorption peak obtained at 1349 and 1348 $cm^{-1}$ from FTIR and FT-Raman spectrum may due to $CH_3$ deformation vibration indicate the presence of methyl ketones. The peaks of different intensities obtained at 1276, 1249 and 1108 $cm^{-1}$ in FTIR spectrum and 1276,1250 and 1106 $cm^{-1}$ in FT-Raman spectrum are due to ring C-H in-plane deformation vibrations. The multiple absorption peaks obtained between the range 900 – 650 $cm^{-1}$confirms the presence of aromatic C-H out of plane bending vibrations [12-15]. The identified intensity peaks in FTIR and FT-Raman spectrum with their particular assignments are tabulated in table 2.

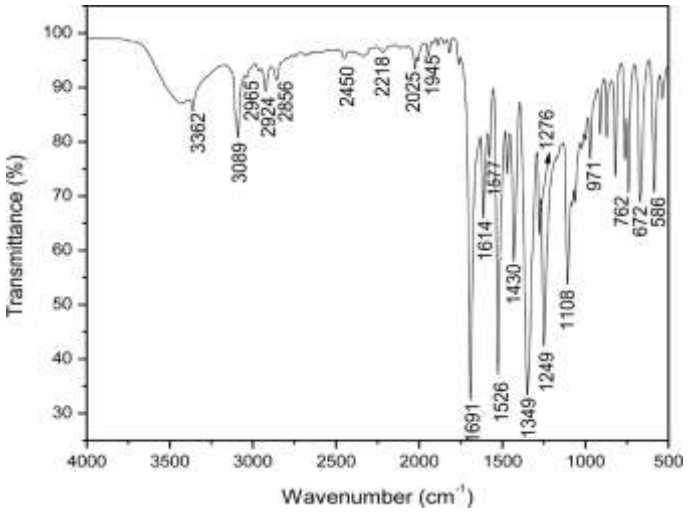


**Fig.4 FTIR spectrum of 3-nitroacetophenone single crystal**

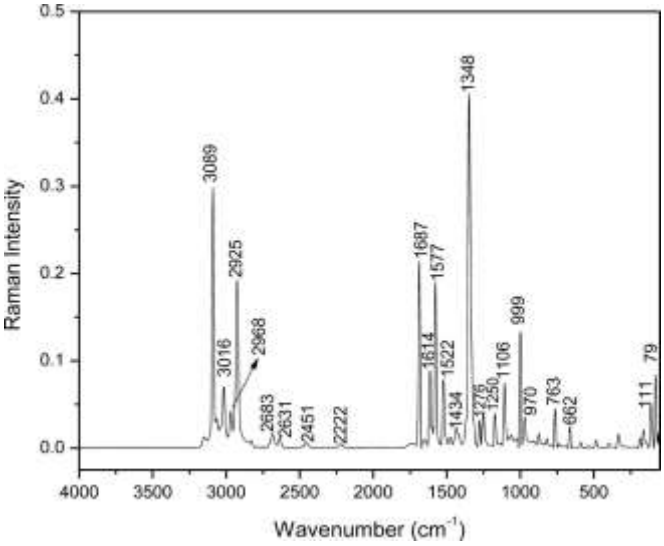


**Fig.5 FT-Raman spectrum of 3-nitroacetophenone single crystal**

**Table 2**

**Molecular Vibrational assignments of 3-nitroacetophenone**

| Wave number($cm^{-1}$) | | | Functional group | Assignments |
|---|---|---|---|---|
| Reference range | FTIR | FT-RAMAN | | |
| 3100-3000 | 3089 | 3089 | Aryl group (=C-H) | CH stretching vibration |
| 3020-2930 | 2965 | 2968 | Methyl ketones ($CH_3$-C=O) | Asymmetric CH stretching vibration |
| 2940-2840 | 2924 | 2925 | Methyl ketones ($CH_3$-C=O) | Symmetric CH stretching vibration |
| 2860-2815 | 2842 | 2844 | Aromatic-methyl (=C-O-$CH_3$) | Symmetric $CH_3$ stretching vibration |
| 1625-1470 | 1614, 1577 | 1614, 1577 | Aromatic -C=C- | Aromatic quadrant ring stretching vibrations |
| 1570-1485 | 1526 | 1522 | Aromatic nitro compounds (N=O) | Asymmetric $NO_2$ stretching vibration |
| 1355-1345 | 1349 | 1348 | Aromatic nitro compounds (N=O) | Symmetric meta substitute $NO_2$ stretching vibration |
| 1330-1180 | 1276, 1249 | 1276, 1250 | Aromatic ring C-H | In-plane deformation vibration |
| 1100-1000 | 1108 | 1106 | Aromatic ring C-H | In-plane deformation vibration |
| 900-650 (several) | 971, 762, 672 | 970, 765, 662 | Aromatic C-H | C-H out of plane bending vibrations |

### 3.3 UV-Vis spectral analysis

The transmittance of the grown 3-nitroacetophenone single crystal was measured at room temperature in the wavelength

range of 200-800 nm by using Perkin-Elmer model: Lambda 35 spectrophotometer. The 3-nitroacetophenone single crystal of 2 mm thickness is used for the analysis. The transmittance versus wavelength plot of the grown crystal is shown in fig. 6(a). The cut-off wavelength was spotted at 382 nm and the crystal shows good transparency. The optical absorption coefficient (α) is a significant parameter used for optical applications . It is calculated by the equation

$$\alpha = \frac{2.303 \log(\frac{1}{T})}{t}$$

Where T is the transmittance and t is the thickness of the grown crystal. The optical band gap ($E_g$) is correlated to absorption coefficient (α) and photon energy (hν) through Tauc relation

$$\alpha h\upsilon = A\left(h\upsilon - E_g\right)^m$$

Where hν is the incident photon energy, A is constant and m denotes the index, which varies according to the mechanism of transition, m = 1/2, 2, 3/2 and 3 for direct allowed, indirect allowed, direct forbidden and indirect forbidden transition. Since the transition here is direct we take m=1/2 and the equation becomes [16,17]

$$\alpha h\upsilon = A\left(h\upsilon - E_g\right)^{1/2}$$

The Tauc plot drawn between $(\alpha h\nu)^2$ and (hν) is shown in fig. 6(b). From the graph, the optical band gap ($E_g$) is found to be 2.83 eV. The absorption coefficient (α) is related to the extinction coefficient (K) by the equation [18]

$$\mathrm{K} = \frac{\lambda\alpha}{4\pi}$$

The graph of extinction coefficient against wavelength is plotted and shown is shown in fig.6(c). The transmittance (T) is given by the equation

$$T = \frac{(1-R)^2 \exp(-\alpha t)}{1 - R^2 \exp(-2\alpha t)}$$

The reflectance (R) in terms of the absorption coefficient (α) is calculated from the equation

$$R = \frac{\exp(-\alpha t) \pm \sqrt{\exp(-\alpha t)\,T - \exp(-3\alpha t)\,T + \exp(-2\alpha t)T^2}}{\exp(-\alpha t) + \exp(-2\alpha t)\,T}$$

By using the calculated reflectance (R) value, the refractive index (n) can be determined by using the formula

$$n = \frac{-(R+1) \pm 2\sqrt{R}}{(R-1)}$$

The graph between refractive index (n) and wavelength (λ) for 3-nitroacetophenone is shown in fig 6(d), which shows that the wavelength increases the refractive index decreases. The optical conductivity ($\sigma_{op}$) which is a measure of the frequency response of the material is given by [19,20]

$$\sigma_{op} = \frac{\alpha n c}{4\pi}$$

Where c is the velocity of light. The dependence of wavelength to optical conductivity of 3-nitroacetophenone is shown in fig 6(e). It shows that the optical conductivity is decreasing as the wavelength increases.

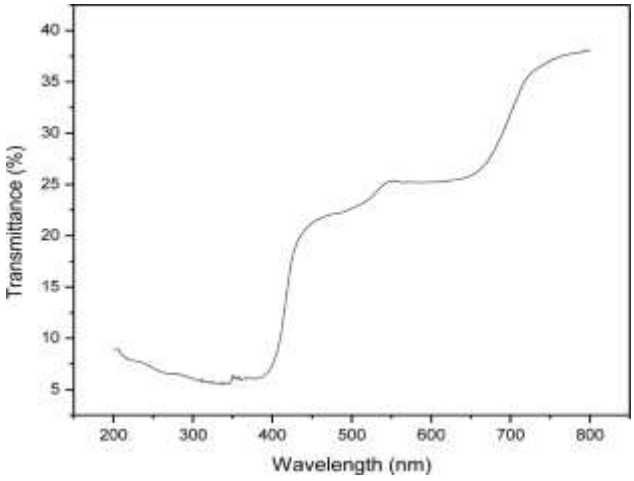


**Fig. 6(a) UV-Vis spectrum of 3-nitroacetophenone single crystal**

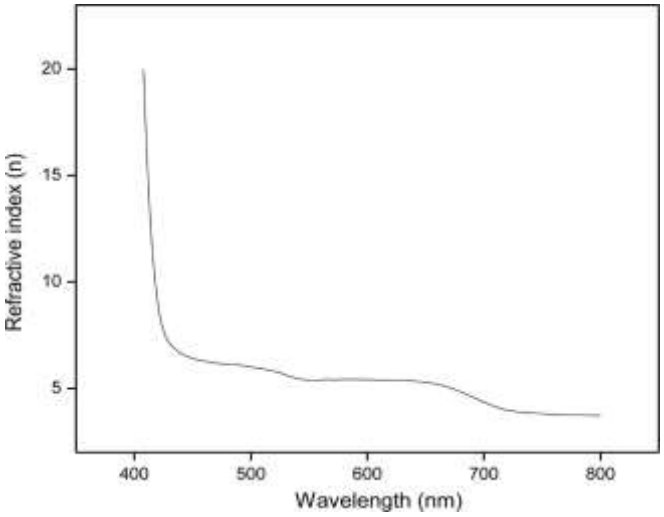


**Fig. 6(b) Tauc plot $(\alpha h\nu)^2$ versus photon energy of 3-nitroacetophenone**

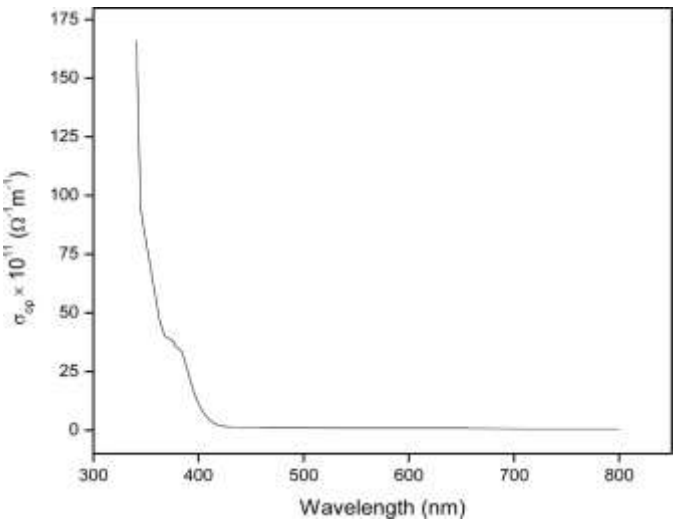


**Fig. 6(c) Plot of extinction coefficient versus wavelength of 3-nitroacetophenone**

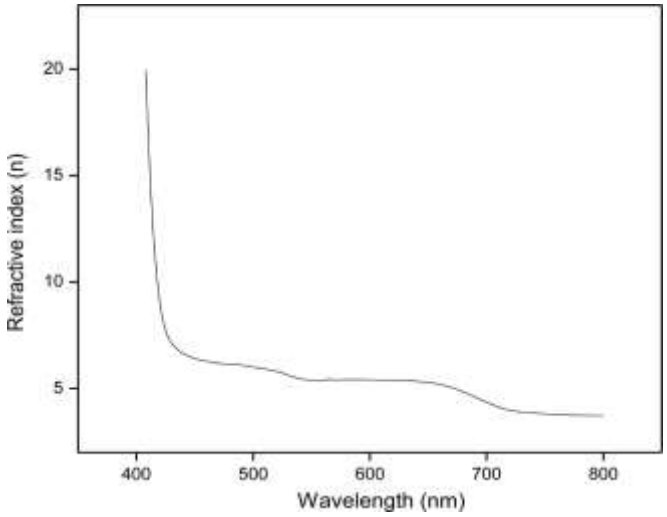


**Fig. 6(d) Plot of refractive index (n) versus wavelength for 3-nitroacetophenone**

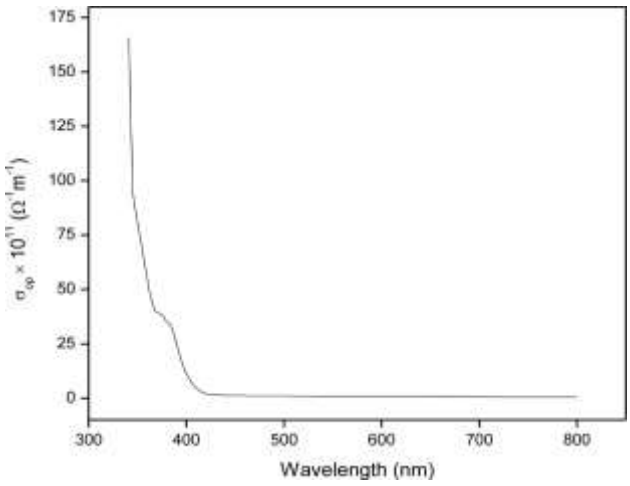


**Fig. 6(e) Optical conductivity versus wavelength curve of 3-nitroacetophenone**

### 3.4 Thermal analysis

Thermogravimetric (TG) and differential thermal analyses (DTA) is used to analyze the thermal stability of the grown 3-nitroacetophenone single crystal. The sample was analyzed simultaneously using SIINT 6300, between the temperature range of 30°C to 500°C at the heating rate of 10°C/min in the nitrogen atmosphere. The recorded TG/DTA curve is shown in fig 7(a). The DTA curve shows two endothermic peaks at 85°C and 238°C. The peak at 85°C is the melting point and no loss of mass in TGA is also been noted. The second endothermic peak at 238°C provides the decomposition point and at this point heavy loss of mass was also observed in the TGA plot. The TGA plot shows single stage decomposition with heavy loss of mass around 238°C, which further leads to determine kinetic parameters.

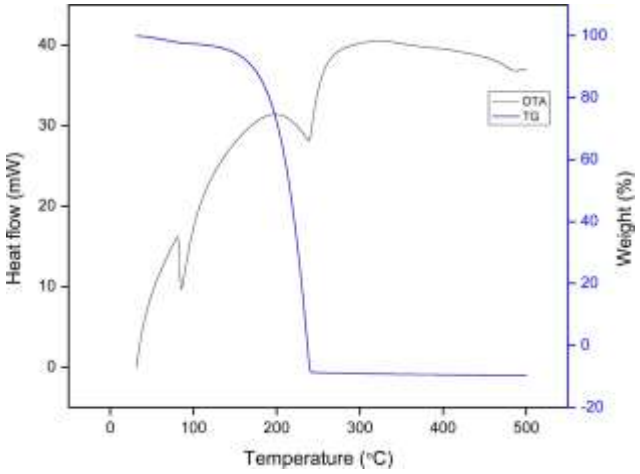


**Fig. 7(a) TG/DTA curve of grown 3-nitroacetophenone single crystal**

The rate constant which depends upon temperature is obtained by Arrhenius equation as

$$\frac{d\alpha}{dt} = A \exp\left(\frac{-E_a}{RT}\right) f(\alpha)$$

Where A is the frequency factor ($sec^{-1}$), $E_a$ is the activation energy ($kJmol^{-1}$), R is the universal gas constant ($J\ mol^{-1}\ K^{-1}$) and T is the absolute temperature. The above equation takes the general integral form

$$g(\alpha) = \int_0^{\alpha} \frac{d\alpha}{f(\alpha)} = A \int_0^{t} exp\left(\frac{-E_a}{RT}\right) dt$$

The time dependence of the above equation is removed by constant heating rate (β□, where β□□□dT/dt. Then the equation takes the form

$$g(\alpha) = \frac{A}{\beta} \int_0^{T} exp\left(\frac{-E_a}{RT}\right) dT$$

This is the preliminary equation used for integral approximation under non-isothermal conditions. The equation is again replaced by $x = E_a/RT$ and the equation takes the form

$$g(\alpha) = \frac{AE_a}{\beta R} \int_x^{\infty} \frac{\exp(-x)}{x^2}\, dx = \frac{AE_a}{\beta R}\, p(x)$$

Where,

$$p(x) = \int_x^{\infty} \frac{\exp(-x)}{x^2}\, dx$$

The three familiar integral approximation methods such as Coats-Redfern, Horowitz- Metzger and Broido are subjected to determine the kinetic parameters activation energy ($E_a$) and frequency factor (A). The exponential integral in the above equation is approximated by Coats-Redfern for n = 1 as [21-23]

$$\ln\left[\frac{g(\alpha)}{T^2}\right] = ln\left[\frac{AR}{\beta E_a}\left(1 - \frac{2RT}{E_a}\right)\right] - \frac{E_a}{RT}$$

The value $ln\left[\frac{AR}{\beta E_a}\left(1 - \frac{2RT}{E_a}\right)\right] = \left(\frac{AR}{\beta E_a}\right)$ remains constant throughout the decomposition process. By linear fitting, the plot of $\ln[g(\alpha)/T^2]$ versus 1000/T and then by taking the slope, the activation energy ($E_a$) is calculated. The curve between $\ln[g(\alpha)/T^2]$ and 1000/T for the Coats-Redfern

method is shown in fig.7(b). Horowitz and Metzger derived the mathematical form of integral approximation using the temperature θ(K) such that θ = T-$T_m$ and generated the equation g(α) for n =1 given by [24,25]

$$\ln g(\alpha) = \frac{E_a \theta}{RT_m^2}$$

$T_m$ represents the peak temperature of the DTA curve. A plot of lng(α) versus θ shown in fig. 7(c) gives the best fit and the slope provides the activation energy ($E_a$) for Horowitz and Metzger method. Broido derived the relation for n = 1 as [26]

$$\ln g(\alpha) = \frac{-E_a}{RT}$$

A plot between ln g(α) and 1000/T is drawn as shown in fig. 7(d). The slope of the straight line obtained from the above graph is used to determine the activation energy ($E_a$). The kinetic parameter activation energy ($E_a$) is calculated by three approximations. By using the obtained activation energy, the frequency factor (A) is calculated using the formula

$$A = \left[\left(\frac{E_a}{RT_m^2}\right)\beta\ exp\left(\frac{E_a}{RT_m}\right)\right]$$

By finding the values of kinetic parameters $E_a$ and A, we can calculate the thermodynamic parameters entropy (ΔS), enthalpy (ΔH) and Gibb's free energy (ΔG) by the following equations using the peak temperature ($T_m$).

$$\Delta S = R \ln\left(\frac{Ah}{k_B T_m}\right)$$

$$\Delta H = E_a - RT_m$$

$$\Delta G = \Delta H - T_m \Delta S$$

Where $k_B$ is Boltzmann constant and h denotes the Planck's constant respectively. The kinetic and thermodynamic parameters are calculated by the three approximation methods for n = 1 and are in good agreement. The negative entropy (ΔS) indicates the more ordered structure of the grown organic single crystal. The positive values of enthalpy (ΔH) and Gibb's free energy (ΔG) shows the endothermic process and the reactions in the decomposition of 3-nitroacetophenone are non-spontaneous. The kinetic and thermodynamic parameters calculated by the three approximation equations are summarized in table 3.

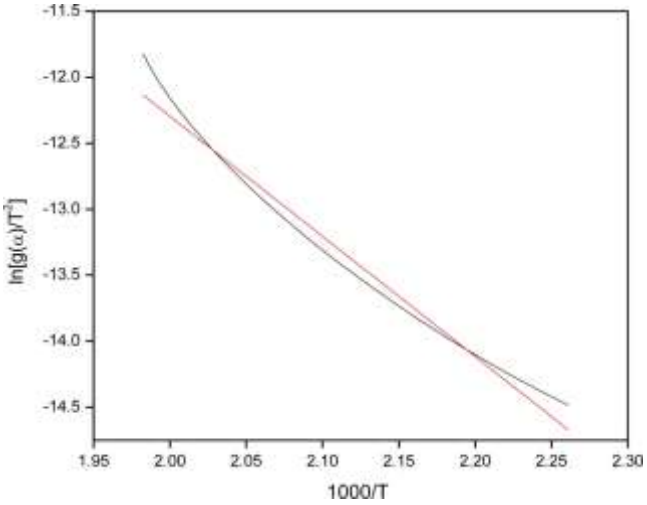


**Fig. 7(b) Coats-Redfern curve of 3-nitroacetophenone single crystal**

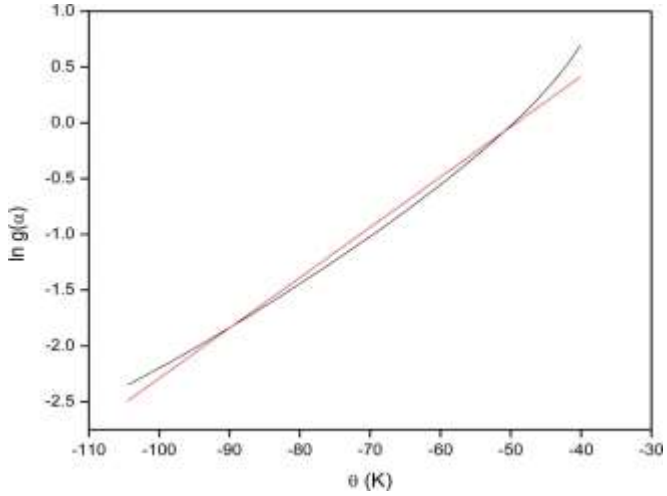


**Fig. 7(c) Horowitz-Metzger curve of 3-nitroacetophenone single crystal**

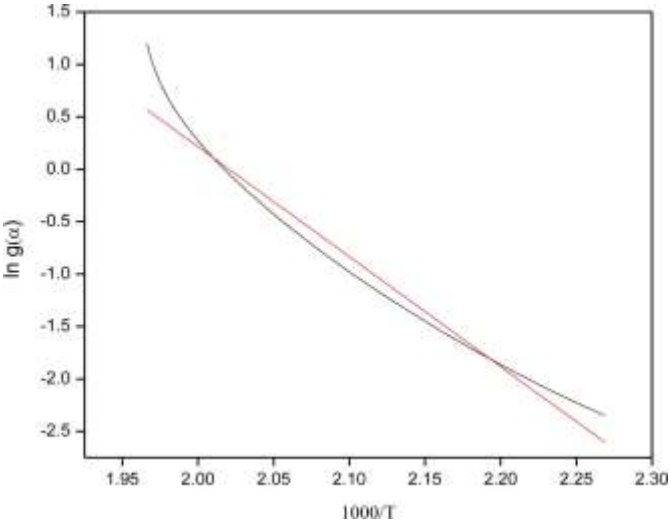


**Fig. 7(d) Broido curve of 3-nitroacetophenone single crystal**

**Table 3**

**Kinetic and Thermodynamic parameters of 3-nitroacetophenone single crystal from the three integral approximation methods**

| Parameters | Coats – Redfern Method | Horowitz-Metzger Method | Broido Method Method |
|---|---|---|---|
| Activation energy (E) (kJ $mol^{-1}$) | 75.66 | 86.70 | 87.13 |
| Frequency factor (A) ($s^{-1}$) | 1.57 x $10^7$ | 1.40 x $10^8$ | 1.55x $10^8$ |
| Entropy (ΔS) (J $K^{-1}$ $mol^{-1}$) | -111.61 | -93.44 | -92.56 |
| Enthalpy (ΔH) (kJ $mol^{-1}$) | 71.41 | 82.45 | 82.88 |
| Gibbs free energy (ΔG) (kJ $mol^{-1}$) | 128.39 | 130.16 | 130.14 |

### 3.5 Dielectric analysis

The dielectric analysis for the grown 3-nitroacetophenone single crystal was done by Agilent 4284A LCR Meter using conventional parallel plate capacitor method [27-28]. The capacitance value and dielectric loss($\tan\delta$) are measured for various temperatures ranging from 313 to 353 K for the frequencies 100 Hz, 1 kHz, 10 kHz, 100 kHz and 1 MHz. The dielectric constant ($\varepsilon_r$) of the grown crystal was calculated using the formula

$$\varepsilon_r = \left[\frac{1}{C_{air}}\right]\left[C_{crys} - C_{air}\left(1 - \frac{A_{crys}}{A_{air}}\right)\right]\left[\frac{A_{air}}{A_{crys}}\right]$$

Where $C_{air}$ is the air capacitance, $C_{crys}$ is the capacitance of the crystal, $A_{crys}$ is the area of crystal in contact with the electrode and $A_{air}$ is the area of electrode. The ac electrical conductivity ($\sigma_{ac}$) was calculated using the relation

$$\sigma_{ac} = \varepsilon_0 \varepsilon_r \omega \tan\delta$$

Where $\varepsilon_o$ is the permittivity of free space ($8.85 \times 10^{-12}$ $C^2$ $N^{-1}$ $m^{-2}$), $\omega$ is the angular frequency ($\omega = 2\pi f$, f is the ac frequency chosen for the analysis) and tan δ is the dielectric loss factor. The variation of dielectric constant, dielectric loss and AC electrical conductivity for different temperature are shown in fig. 8 (a-c). The figure reveals that the dielectric constant, dielectric loss and AC electrical conductivity increases as the temperature increases. The high dielectric constant attained at low frequency is due to the role of space charge, orientational, ionic and electronic polarization and low dielectric constant at high frequency attained may be due to the gradual loss of polarization. The low dielectric constant ($\varepsilon_r$) and dielectric loss (tan δ) at high frequencies shows the less defect and good optical quality of the grown 3-nitroacetophenone single crystal, it may be used for the fabrication of nonlinear optical devices [27-30]. The activation energy of the grown crystal was calculated from Arrhenius plot using the relation.

$$\sigma_{ac} = \sigma_0 \, exp\left(\frac{-E_a}{kT}\right)$$

$\sigma_{ac}$ denotes the electrical conductivity at the particular temperature , $\sigma_0$ is the pre-exponential factor, $E_a$ is the activation energy, k is the Boltzmann constant and T is the absolute temperature. The activation energy is calculated by the slope of the Arrhenius plot drawn between ($\sigma_{ac}$) and 1/T. The slope from the graph is ($-E_a/k$) and hence the above equation can be written as

$$\ln\sigma_{ac} = \ln\sigma_0 + slope\left(\frac{1}{T}\right)$$

The slope which is in negative value is figured out from the plot drawn between ln ($\sigma_{ac}$) and 1/T, which is further used to calculate the activation energy as

$$E_a = -k \times slope$$

The activation energy obtained for various frequencies are 0.2996, 0.2647, 0.1772, 0.0962, 0.0798 eV. The activation energy $E_a$ decreases as the frequency increases, indicating that the bounding conduction is the principal mechanism [31, 32]. The dielectric analysis is further used to determine the valence electron plasma energy and an average energy gap known as Penn gap and Fermi energy.

$$\hbar\omega_P = 28.8\left(\frac{Z\rho}{M}\right)^{1/2}$$

Z denotes the total number of valence electrons. The density (ρ) and molecular weight (M) of the grown 3-nitroacetophenone is 1.407 g/cm$^3$ and 165.15 g/mol. Using the relevant dielectric constant in the plasmon energy, the Penn gap can be determined. The Penn gap is found by using the formula [33-35]

$$E_P = \frac{\hbar\omega_P}{(\varepsilon_r - 1)^{1/2}}$$

Fermi energy is calculated by the following formula

$$E_F = 0.2948(\hbar\omega_P)^{4/3}$$

$E_P$ is the Penn gap, $E_F$ is the Fermi energy , $\hbar\omega_p$ is the valence electron plasma energy and $\varepsilon_r$ is the dielectric constant of the grown crystal at 1 kHz frequency. The electronic polarizability (α) is calculated by three methods and are compared.

Using the valence electron plasma energy α is given by

$$\alpha = \left[\frac{(\hbar\omega_P)^2 S_0}{(\hbar\omega_P)^2 S_0 + 3E_P^2}\right] \times \frac{M}{\rho} \times 0.396 \times 10^{-24} cm^3$$

Where $S_0$ is a constant given by,

$$S_0 = 1 - \left(\frac{E_P}{4E_F}\right) + \frac{1}{3}\left(\frac{E_P}{4E_F}\right)^2$$

Using the Clausius-Mossotti equation, α is given by

$$\alpha = \left(\frac{3M}{4\pi N_a \rho}\right)\left(\frac{\varepsilon_r - 1}{\varepsilon_r + 2}\right)$$

Where $N_a$ is the Avogadro number ($N_a = 6.023 \times 10^{23}$)

The following empirical relationship is used to calculate α

$$\alpha = \left(1 - \frac{\sqrt{E_g}}{4.06}\right) \times \frac{M}{\rho} \times 0.396 \times 10^{-24} \text{cm}^3$$

Where $E_g$ is the optical band gap (eV). The calculated electronic parameters plasma energy, Penn gap, Fermi energy and electronic polarizability for the grown single crystal values are shown in Table 4.

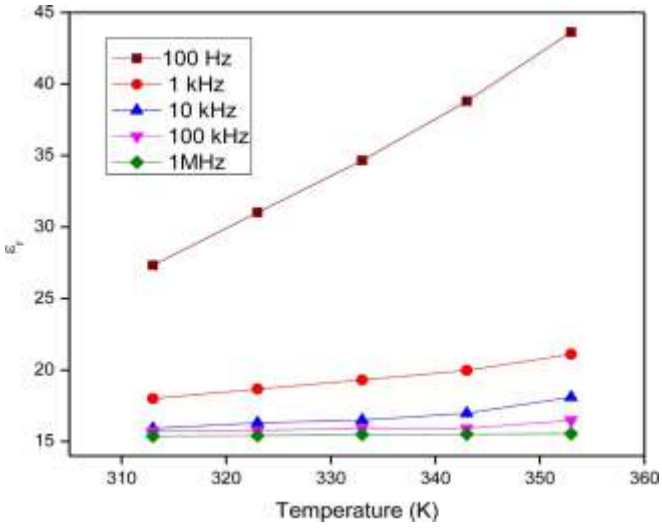


**Fig. 8(a) Dielectric constant versus temperature graph of 3-nitroacetophenone**

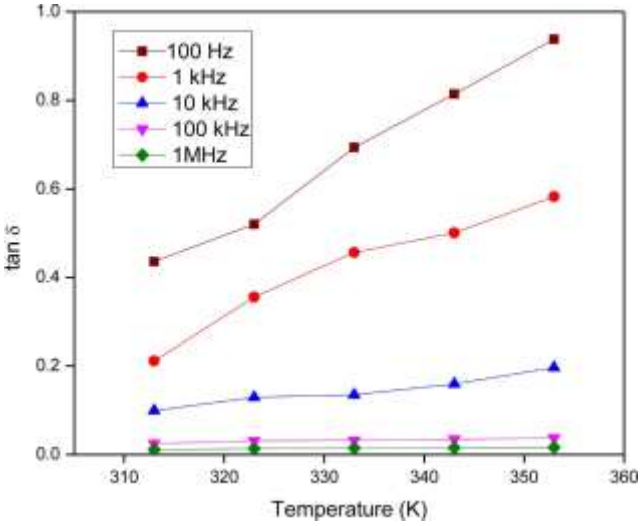


**Fig. 8(b) Dielectric loss versus temperature graph of 3-nitroacetophenone**

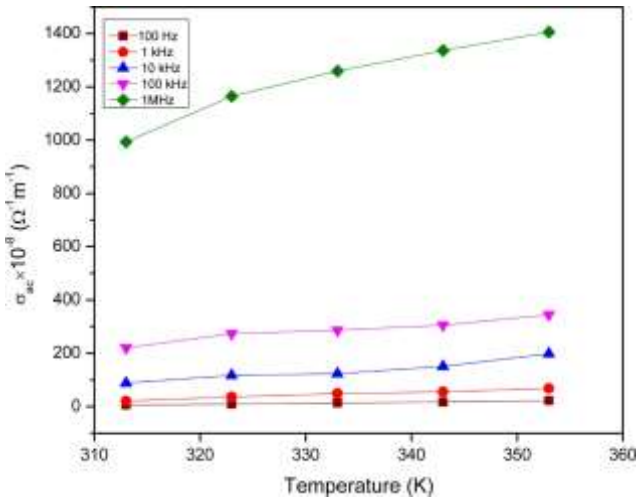


**Fig. 8(c) AC electrical conductivity versus temperature plot of 3-nitroacetophenone**

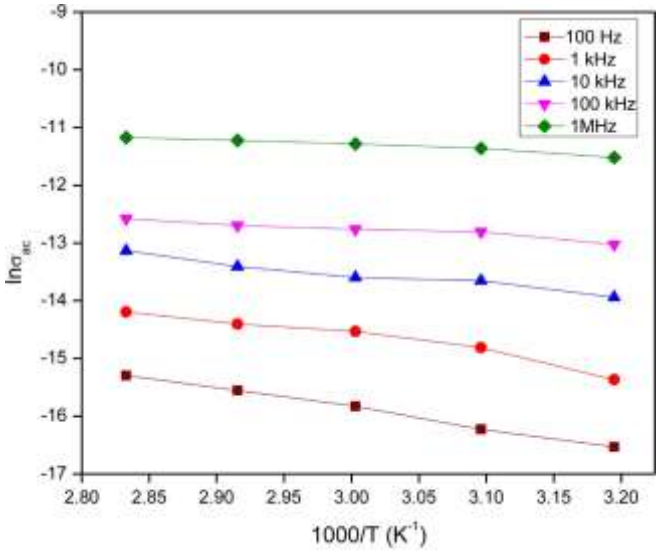


**Fig. 8(d) Plot of $\ln\sigma_{ac}$ versus 1000/T for 3-nitroacetophenone**

**Table 4**

**Electronic parameters for 3-nitroacetophenone single crystal**

| Parameter | Calculated values |
|---|---|
| Plasma energy $\hbar\omega_p$ (eV) | 20.931 eV |
| Penn gap $E_P$ (eV) | 5.075 eV |
| Fermi energy $E_F$ (eV) | 17.005 eV |
| Electronic polarizability α ($cm^3$) | |
| From Penn analysis | $3.905 \times 10^{-23}$ $cm^3$ |
| From Clausius-Mossotti equation | $3.956 \times 10^{-23}$ $cm^3$ |
| From optical band gap | $2.722 \times 10^{-23}$ $cm^3$ |

## 4.Conclusion

The organic 3-nitroacetophenone single crystal was grown using acetone as solvent by slow evaporation technique at room temperature. The lattice parameter is identified by single crystal XRD and powder XRD analyses, which shows the good crystalline nature of the grown crystal. The functional groups present in the grown crystal were spotted by FTIR and FT-Raman analyses. The grown crystal has good transparency in the visible region. The TG/DTA study shows that the crystal possesses good thermal stability. Coats-Redfern, Horowitz-Metzger and Broido integral approximation methods are used to calculate the kinetic and thermodynamic parameters. The dielectric analysis shows that the grown crystal has normal dielectric characteristics. The electronic parameters like Plasma energy ($\hbar\omega_p$), Penn gap ($E_P$), Fermi energy ($E_F$) and electronic polarizability (α) were calculated.

## References


1. Song Chen, Ming-Peng Zhuo, Xue-Dong Wang, Guo-Qing Weiand Liang-Sheng Liao, PhotoniX ,2,2 (2021)
2. R. Santhakumari, K. Ramamurthi, G. Vasuki, Bohari M. Yamin, G. Bhagavannarayana, Spectrochimica Acta Part A, 76, 369–375 (2010)
3. S. Sasi, R. Uthrakumar, S. Arumugam, R. Robertand C. Inmozhi, Elixir Crystal Research 75, 27559-27561 (2014)
4. AkichikaKumatani, Chuan Liu, Yun Li, Peter Darmawan, Kazuo Takimiya, Takeo Minari & KazuhitoTsukagoshi, Sci. Rep., 2, 393 (2012)
5. Sirringhaus. H, Adv. Mater., 17, 2411–2425(2005)
6. J.Cornil, J.Ph.Calbert and J.L.Bredas, J. Am. Chem. Soc., 123, 1250-1251 (2001)
7. Adams,J.P.J.Chem.Soc.PerkinTrans.I.2002,23,2586–2597.
8. BetulCaliskan and Ali Cengiz Caliskan, Radiat. Eff. Defects Solids, 1-13 (2017)
9. Mahendra Kumar Trivedi, Rama Mohan Tallapragada, Alice Branton, Dahryn Trivedi, Gopal Nayak, Rakesh

Kumar Mishra, Snehasis Jana, Science Journal of Analytical Chemistry, 3, 6, 71-79 (2015)

10. N. Feeder, W. Jones, A.P. Chorlton and R. Docherty, Acta Cryst., C52, 1454-1456 (1996)
11. Modern Raman Spectroscopy – A Practical Approach, Ewen Smith, Geoffrey Dent, John Wiley & Sons Ltd, England (2005)
12. G.Socrates, Infrared and Raman characteristic group frequencies: Tables and charts, (John Wiley and sons Ltd, Chichester, 2001)
13. John Coates, Interpretation of Infrared Spectra - A Practical Approach, (John Wiley & Sons Ltd, Chichester, 2000)
14. Lynnette Joseph, D. Sajan, K. Chaitanya, T. Suthan, N.P. Rajesh, Jayakumary Isac, Spectrochimica Acta Part A, 120, 216-227 (2014)
15. B.S. Arun Sasi, R.P. Jebin, T. Suthan, C. James, J. Mol. Struct. 1146, 797-807 (2017)
16. J.W. Jeon, D.W. Jeon, T. Sahoo, M. Kim, J.H. Baek, J. L. Hoffman, N. S. Kim and I.H. Lee, Journal of Alloys and Compounds, 509, 10062 – 10065(2011)
17. M. Loganayaki, A. Senthil, P. Murugakoothan, Int. J. Comput. Appl, 72, 0975 – 8887 (2013)
18. Zhu, J, Zhao S, Xiao D, Wang X, Xu G, J. Phys. Condens. matter., 4, 2977 (1992)
19. R.P. Jebin, T. Suthan, T.R. Anitha, N.P. Rajesh, G. Vinitha, J. Mater. Sci.: Mater. Electron. 32 (3), 3232-3246 (2021)
20. S. Prince, T. Suthan, C. Gnanasambandam, J. Electron. Mater. (2022) https://doi.org/10.1007/s11664-022-09428-7
21. R. Ebrahimi-Kahrizsangi, M. H. Abbasi, Trans. Nonferrous Met. Soc. China, 18, 217-221 (2008)
22. Chen H J, Lai K M, J of Chem. Eng. Of Japan, 37, 9, 1172−1178 (2004)
23. Coats A V, Redfern J P, Nature, 201, 68−69 (1964)
24. R Vini, S Thenmozhi and SC Murugavel, High performance polymers, 31, 86-96 (2018)
25. Vineeta Gupta, K.K.Bamzai, P.N.Kotru, B.M.Wanklyn, materials science and engineering, 130, 163-172 (2006)
26. A. Broido, Journal of polymer science, 7, 1761-1773 (1969)
27. T. Suthan, P.V. Dhanaraj, N.P. Rajesh, C.K. Mahadevan, Cryst. Eng. Comm. 13 (12), 4018-4024 (2011)
28. T. Suthan, N.P. Rajesh, J. Cryst. Growth 312 (21), 3156-3160 (2010)
29. Suresh Sagadevan and Priya Murugasen, International journal of materials and Engineering, 3, 159 – 166 (2015)
30. R.P. Jebin, T. Suthan, N.P. Rajesh, G. Vinitha, Optics and Laser Technology 115, 500– 507 (2019)
31. U. S. Army, Nanostruct Mater. 4, 985-1009 (1994)
32. S. Prince, T. Suthan, C. Gnanasambandam, N.P. Rajesh, G. Vinitha, J. Mater. Sci.: Mater. Electron. (2022) https://doi.org/10.1007/s10854-022-07772-2
33. C. Besky Job, J. Anbuselvam, R.Shabu, S.PaulRaj, International journal of Chem tech research, 8, 250-259 (2015)
34. S. Siva Bala Solanki, N. P. Rajesh, T. Suthan, J. Mater. Sci.: Mater. Electron. 32, 1808–1817 (2021)
35. S. Siva Bala Solanki, N.P. Rajesh, T. Suthan, Optics and Laser Technology 103, 163–169 (2018)

**Compliance with Ethical Standards**

Disclosure of potential conflicts of interests.

**Competing Interests**

No conflict of interest exists, or if such conflict exists, the exact nature must be declared.

**Research Data Policy and Data Availability Statements**

All data generated or analysed during this study are included in this manuscript.

**Author Contributions**

All authors contributed to the study conception and design. Material preparation, data collection and analysis were performed by all authors. All authors read and approved the final manuscript.